Size Separation of Single-Wall Carbon Nanotubes by Flow-Field Flow Fractionation

ARTICLE *in* ANALYTICAL CHEMISTRY · MAY 2008

Impact Factor: 5.64 · DOI: 10.1021/ac7023624 · Source: PubMed

4 AUTHORS, INCLUDING:

Jaehun Chun
Pacific Northwest National Laboratory
45 PUBLICATIONS **912** CITATIONS
SEE PROFILE

E. K. Hobbie
North Dakota State University
163 PUBLICATIONS **2,974** CITATIONS
SEE PROFILE

Anal. Chem. **2008,** *80,* 2514−2523

Size Separation of Single-Wall Carbon Nanotubes by Flow-Field Flow Fractionation

Jaehun Chun, Jeffrey A. Fagan, Erik K. Hobbie, and Barry J. Bauer*

Polymers Division, National Institute of Standards and Technology Gaithersburg, Maryland 20899

Flow-field flow fractionation (flow-FFF) is used to separate single wall carbon nanotubes (SWNTs) dispersed in aqueous medium by the use of DNA. Online measurements are made of SWNT concentration, molar mass, and size by using UV−vis absorption and multiangle light scattering (MALS). Separations are made of both unfractionated SWNTs and SWNT fractions made by use of size exclusion chromatography (SEC). The SEC fractions are well resolved by flow-FFF. SWNT hydrodynamic volume from calibrations with polymer latex particles in flow-FFF are compared to calibrations of hydrodynamic volume from the SEC fractions derived from dissolved polymers. Rod lengths of the SWNTs are calculated from online measurements of MALS and those are compared to rod lengths from hydrodynamic models based on latex sphere calibrations. Samples with varied sizes were prepared by fracturing SWNTs through extended sonication. Flow-FFF of these fractured samples shows very broad size distributions compared to the original SEC and flow-FFF fractions.

Single wall carbon nanotubes (SWNTs) are rodlike molecular objects whose length and diameter are about 100−1000 nm and 0.5−2 nm, respectively. They have the structure of a rolled graphene sheet, and direction and magnitude of a roll-up vector determine the chirality and diameter. Because of unique mechanical and electrical properties, SWNTs have been proposed for many potential applications such as high strength and conductive composites, energy storage, sensors, field emission displays, radiation sources, hydrogen storage media, and nanometer-sized semiconductor devices.[1] SWNTs usually exhibit distributions of length, chirality, and diameter in the as-produced material. However, separation of SWNTs by those characteristics (i.e., length, chirality, and diameter) still remains a challenge and thus defers many practical applications.

Separation of SWNTs by length is especially important not only because the length is associated with optical properties[2] and quantum yields[3] but also because it may be necessary as a preliminary step for separation by chirality.[4,5] Separation of SWNTs by length can be achieved through several approaches, size exclusion chromatography (SEC), gel electrophoresis (GE), capillary electrophoresis (CE), or field flow fractionation (FFF). Recent studies have shown that SEC can produce reasonable resolution of SWNTs by length.[5−7] However, the exclusion limit of the SEC column, controlled by the pore size, restricts the maximum length SWNTs (<1 μm) that can be separated. On the basis of atomic force microscopy (AFM) measurements, Doorn et al.[8] showed that CE can be used to separate SWNTs by length but the length distributions of their fractions are very broad and the quantity separated is extremely small. Whereas several studies have used FFF to separate surfactant dispersed SWNTs, little analytical information is available on their separations.[9−11] Moreover, those studies did not use dispersants that effectively separate single SWNTs from bundles.

We employ flow-field flow fractionation (flow-FFF), equipped with online multiangle light scattering (MALS) and UV−vis photodiode array (PDA), to give a convincing demonstration of separation of SWNTs by length and to use flow-FFF as an analytical tool for the characterization of SWNTs. SWNT/DNA length fractions produced by SEC are used to measure the efficiency of flow-FFF separations. The separations are calibrated by the use of latex particles of known dimensions, and the separation mechanisms of flow-FFF and SEC are compared. The analytical capabilities of FFF are demonstrated with examples of the measurement of relative size distributions from FFF, SEC, and SWNT fracturing.

Flow-FFF of Rodlike Molecules. Flow-FFF has become a widely used technique for size separation of various nanoparticles and macromolecules such as polymer latexes and proteins, taking advantage of a balance between random thermal and uniform flow-driven motions on the object of interest.[12] Flow-FFF uses two parallel plates separated by less than 1 mm. A fluid is caused to flow between the plates, and a parabolic flow profile is established. One of the plates is made from a porous membrane that allows

* To whom correspondence should be addressed. Phone: 301-975-6849. Fax: 301-975-4924. E-mail: barry.bauer@nist.gov.

(1) Baughman, R. H.; Zakhidov, A. A.; de Heer, W. A. *Science* **2002**, *297*, 787.
(2) Fagan, J. A.; Simpson, J. R.; Bauer, B. J.; Lacerda, S. H.; Becker, M. L.; Chun, J.; Migler, K. B.; Hight Walker, A. R.; Hobbie, E. K. *J. Am. Chem. Soc.* **2007**, *129*, 10607.
(3) Crochet, J.; Clemens, M.; Hertel, T. *J. Am. Chem. Soc.* **2007**, *129*, 8058.
(4) Zheng, M.; Jagota, A.; Strano, M. S.; Santos, A. P.; Barone, P.; Chou, S. G.; Diner, B. A.; Dresselhaus, M. S.; Mclean, R. S.; Onoa, G. B.; Samsonidze, G. G.; Semke, E. D.; Usrey, M.; Walls, D. J. *Science* **2003**, *302*, 1545.
(5) Zheng, M.; Semke, E. D. *J. Am. Chem. Soc.* **2007**, *129*, 6084.
(6) Farkas, E.; Anderson, M. E.; Chen, Z.; Rinzler, A. G. *Chem. Phys. Lett.* **2002**, *363*, 111.
(7) Huang, X.; Mclean, R. S.; Zheng, M. *Anal. Chem.* **2005**, *77*, 6225.
(8) Doorn, S. K.; Fields, R. E., III; Hu, H.; Hamon, M. A.; Haddon, R. C.; Selegue, J. P.; Majidi, V. *J. Am. Chem. Soc.* **2002**, *124*, 3169.
(9) Chen, B.; Selegue, J. P. *Anal. Chem.* **2002**, *74*, 4774.
(10) Moon, M. H.; Kang, D.; Jung, J.; Kim, J. *J. Sep. Sci.* **2004**, *27*, 710.
(11) Tagmatarchis, N.; Zattoni, A.; Reschiglian, P.; Prato, M. *Carbon* **2005**, *43*, 1984.
(12) Giddings, J. C. *Unified Separation Science*; Wiley-Interscience Publication: New York, 1991.

10.1021/ac7023624 CCC: $40.75
Published on Web 02/27/2008

the fluid carrier to pass through but retains all larger eluents from passing through. This causes a flow field to be established. For a specific particle diffusion coefficient and hence size, a balance is established which gives rise to a steady-state concentration profile with an average characteristic length (i.e., an equilibrium distance l_c) near an accumulation wall in the flow channel. Combined with a nonuniform velocity field, these differences in position result in different elution times. Given this flow-FFF mechanism, a small particle elutes earlier than a large particle.

For flow-FFF with SWNTs, which can have extremely large aspect ratios, the rotational dynamics of a rodlike particle may also need to be considered in addition to the vertical position of the SWNT center of mass. These dynamics would be important if the rodlike nature of the SWNT invokes a steric (or wall exclusion) mechanism associated with the SWNT length; the mechanism could cause a problem with the separation of longer SWNTs. For spheres in fact, the elution time is reversed for a larger particle due to a steric mechanism when the equilibrium distance l_c becomes comparable to particle radius.[12]

Under a shear flow in a Newtonian fluid, a rodlike particle tends to align with the flow direction, which can be described by the Jeffery orbit.[13] The characteristic residence time of an aligned configuration scales as $O(\gamma/\Gamma)$ where γ and Γ represent the aspect ratio of a rodlike particle and a local shear rate, respectively. Whereas this is correct for any rodlike particle, Brownian motion always exists and randomizes a Jeffery orbit. A tendency to follow the orbit can be represented by the rotary Peclet number for a rod, i.e., $Pe_r = \pi\mu L^3\Gamma/3kT(\ln \gamma - 0.8)$, where μ is viscosity of suspending medium, k is the Boltzmann constant, L is a length of rodlike particle, and T is temperature.[14] When $Pe_r \gg 1$, the particle follows a Jeffery orbit, and when $Pe_r \ll 1$, a random orientation occurs.

Typically in flow-FFF, the equilibrium distance l_c decreases with increasing L, as the translational diffusion coefficient decreases with the increasing length of the particle.[14] An important question here is whether the length of the rod will be a relevant length scale for the steric mechanism, which might be the case when random Brownian motion dominates. We show that the steric mechanism is associated only with the diameter of the rod, rather than length, because Pe_r increases near the accumulation wall of the channel. Whereas Pe_r for a rod of 1 μm in length is still about $O(1)$ under unbounded circumstances, the hydrodynamic interaction between the accumulation wall of the channel and the particle is expected to increase significantly as the separation approaches or becomes less than $L/2$. This interaction will increase the "effective" Pe_r.[15] Equating l_c to $L/2$ enables us to approximate a critical length (L_{cri}) above which a rodlike particle will become aligned due to the hydrodynamic interaction: $L_{cri} \approx \sqrt{2kT\ln\gamma/3\pi\mu\langle U_{cross}\rangle}$. Implementation of typical experimental conditions (i.e., $\langle U_{cross}\rangle = 6.9 \times 10^{-6}$ m/s) along with an approximation of $\sqrt{\ln\gamma/\pi} \approx 1$ over the length range of interest, it can be deduced that SWNTs may start to align parallel to an accumulation wall of the channel beyond approximately 600 nm in length. This simple argument implies that one can ignore the steric mechanism for the separation of most longer SWNTs because the steric mechanism becomes effective only at an equilibrium distance comparable to the diameter of the SWNT (i.e., about 1 nm), owing to the alignment of the SWNT.

(13) Jeffery, G. B. *Proc. R. Soc. London, Ser. A* **1922**, *102*, 161.
(14) Doi, M.; Edwards, S. F. *The Theory of Polymer Dynamics*; Oxford University Press: New York, 1986.
(15) Nitsche, J. M.; Roy, P. *AIChE J.* **1996**, *42*, 2729.

EXPERIMENTAL SECTION

The measurements presented here were performed on SWNTs prepared by the cobalt−molybdenum catalyst (CoMoCAT) process, but analogous behavior was also measured for SWNTs grown with the high-pressure carbon monoxide (HiPco), laser ablation, and electric arc methods. Aqueous dispersions of CoMoCAT SWNTs (batch NI-6-A001 S-P95-02, Southwest Nanotechnologies Inc.) in the presence of 30-mer 5′-GT(GT)$_{13}$GT-3′ single stranded DNA (Integrated DNA Technologies) were prepared by following the method of Zheng et al.[16] A standard sample preparation is sonication in an ice water bath (10 W, 3.2 mm tip sonicator) of 1 mg/mL SWNTs in salt solution (0.2 mol/L of NaCl, 0.04 mol/L of Tris(hydroxymethyl)aminomethane, 200 μg/g of NaN_3, HCl to pH = 7.0) with 1 mg/mL of the single stranded DNA for 2 h, followed by centrifugation (2 h, 21 000*g*). SWNT fractions having different lengths were obtained from our previous SEC experiments; they were collected at 2 min intervals, and the first (i.e., longest) fraction was designated fraction 5 and successively shorter nanotubes were collected in following fractions up to fraction 16.[2,17,18] Two additional samples were prepared in an identical manner except that the total sonication times were 14 and 27 h. The unattached DNA is quantitatively removed from solution, but the attached DNA is strongly bound and does not significantly dissociate from the SWNTs over extended periods of time.[17]

Separations were made with a flow-FFF system (Eclipse 2, Wyatt Technologies) equipped with a programmable pump (Isocratic 1200, Agilent Technologies), flow controller, and flow channel equipped with a 10 kDa regenerated cellulose membrane and 350 μm thickness spacer (Wyatt Technology). Online detection used multiangle light scattering (Dawn EOS, Wyatt Technology), UV−vis spectroscopy (2487 dual λ absorbance detector, Waters), photodiode array detector (2996, Waters), and a refractive index meter (Optilab, Wyatt Technology). Fluorescence interference in the MALS was eliminated by the use of filters over half of the available detectors, and six detectors were used for the data analysis. A forward laser monitor was used to measure the absorption of the 690 nm incident beam. Astra Software (Wyatt Technology) was used to collect the MALS and UV−vis absorbance and to correct for laser absorption at the scattering volume. Absolute scattering intensity was calculated based on Rayleigh scattering from toluene, and MALS detector sensitivity was calibrated with narrow poly(methacrylic acid) standards. The data were output and fit as described in a later section. UV−vis spectroscopy at 690 nm was used to measure SWNT concentrations because minimal length dependence of absorbance takes place at this wavelength for the CoMoCat SWNTs.[2] The flow profile was most commonly 2 min of an initial focusing step, 200 μL SWNT injection into the flow channel over 3 min, followed by

(16) Zheng, M.; Jagota, A.; Semke, E. D.; Diner, B. A.; Mclean, R. S.; Lustig, S. R.; Richardson, R. E.; Tassi, N. G. *Nat. Mater.* **2003**, *2*, 338.
(17) Bauer, B. J.; Fagan, J. A.; Hobbie, E. K.; Chun, J.; Bajpai, V. *J. Phys. Chem. C*, **2008**, *112*, 1842−1850.
(18) Bauer, B. J.; Becker, M. L.; Bajpai, V.; Fagan, J. A.; Hobbie, E. K.; Migler, K.; Guttman, C. M.; Blair, W. R. *J. Phys. Chem. C* **2007**, *111*, 17914.

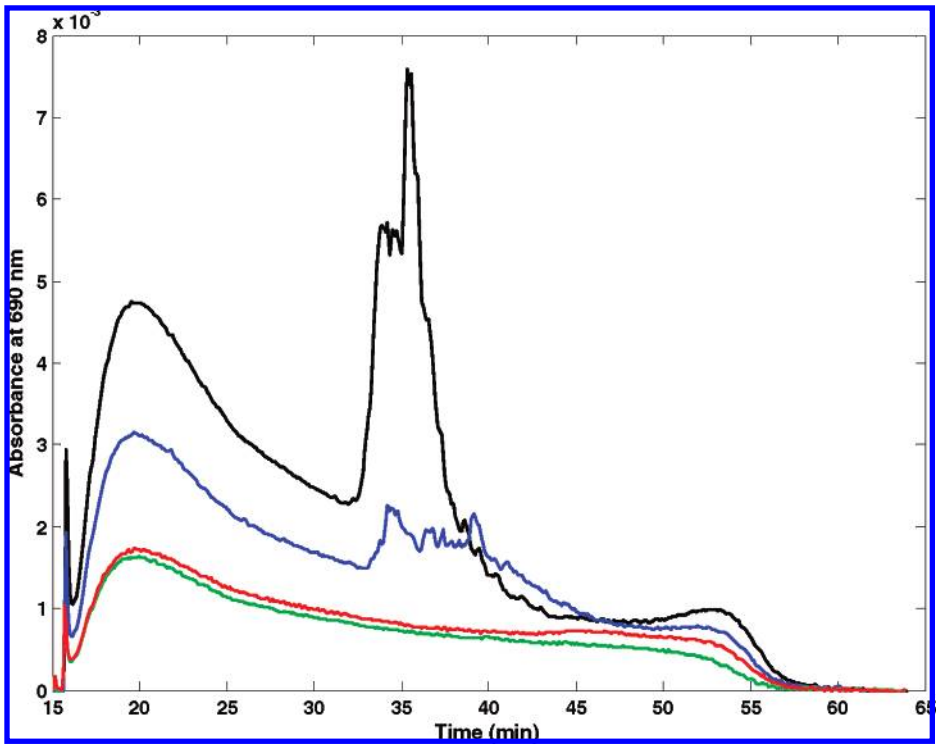

Figure 1. Flow FFF elution profiles for four different SWNT/DNA suspensions modified by both filtration and dilution. Black and blue curves correspond to SWNT/DNA suspensions with a typical concentration of SWNTs: unfiltered (black) and filtered (blue). Red and green curves denote about a 3 times dilution of SWNT/DNA suspensions in comparison to that of a typical concentration: unfiltered (red) and filtered (green).

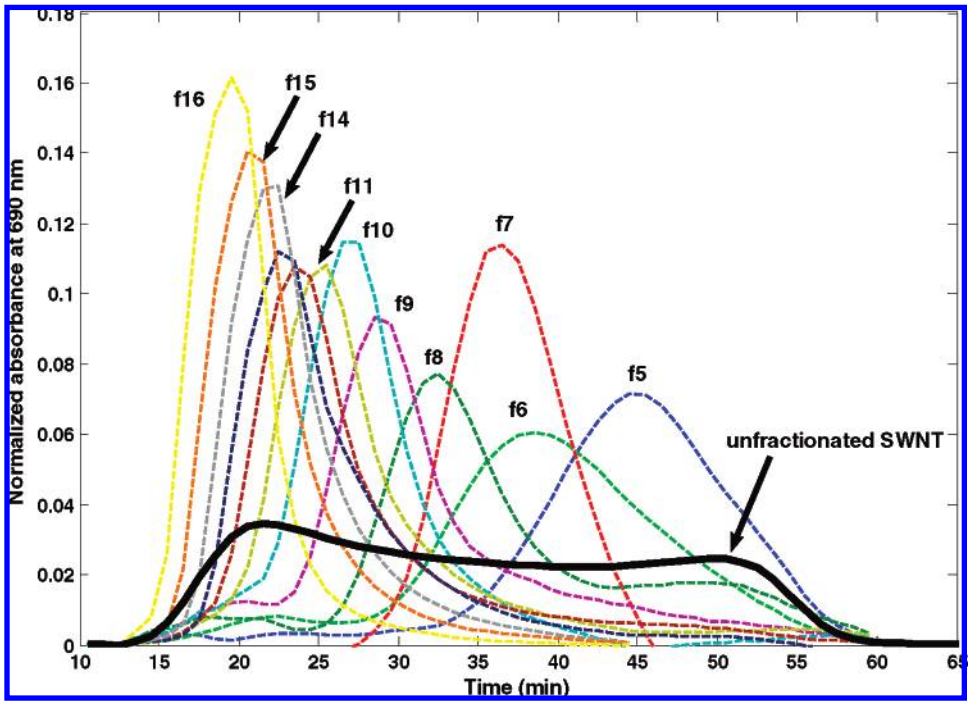

Figure 2. Flow FFF elution profiles for 12 different SEC fractions and corresponding unfractionated SWNT/DNA. All fractions were previously obtained from our SEC experiments.[2,17,18] Normalization is based on area to show the relative broadness of each fraction peak. Note that notations for fraction 12 and 13 are omitted for the sake of space.

a sample focusing step of 10 min. A volumetric channel flow rate was set to 1.0 mL/min, and a volumetric cross-flow rate was initially set to 1.4 mL/min and decreased to zero in 40 min. The mobile solution in the experiments was the same as the salt solution described above.

Certain equipment, instruments or materials are identified in this paper in order to adequately specify the experimental details. Such identification does not imply recommendation by the National Institute of Standards and Technology nor does it imply the materials are necessarily the best available for the purpose.

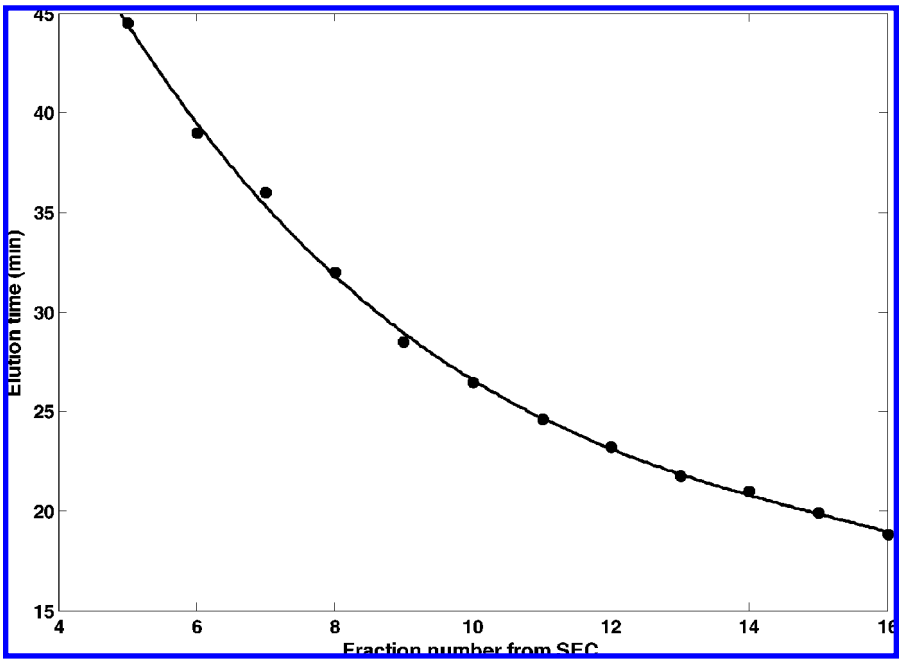

Figure 3. Flow FFF elution times of 12 different SEC fractions, where the curve is intended as a guide to the eye. The slope of the curve is greater when the SEC fractions are eluted through FFF over a longer time, resulting in a broader elution profile.

RESULTS AND DISCUSSION

Optimization of Separations. The flow-FFF separation was optimized for DNA dispersed SWNT samples by varying sample concentration and flow programming. Figure 1 shows absorbance of unfractionated SWNT/DNA at 690 nm for four different sample preparation methods. (In all figures with symbols, error bars representing 1 standard deviation are shown only when larger than the symbol; in figures with lines error bars are commensurate with indicated scatter.) We caution that using SWNT/DNA suspensions with a typical concentration for SEC separations (0.4 mg/mL) and a 200 μL sample loop (compared to 500 μL for SEC) resulted in flow instabilities that cause poor separations. When injecting these concentrations, the focusing step produces a sharp line of SWNTs that can be easily seen through the transparent upper channel. Upon initiation of the channel flow, the expected broadened band appears and moves down the channel. However, a small erratic flow of dark material (i.e., fingering) also appears in the channel. The large ragged peak in the black curve of Figure 1 is the response of the absorption detector to this flow. When the as-prepared sample is filtered, the concentration decreased to 0.27 mg/mL as determined by integration of the 690 nm absorbance. Figure 1 shows that there are still some anomalous signals under this condition (i.e., blue curve). Both the unfiltered and filtered samples were then diluted to 0.15 and 0.13 mg/mL, respectively. The absorbance of these two samples no longer displays the flow instabilities of the higher concentrations. The concentration of the samples is thus clearly limited by this effect. The total amount of SWNT per injection is 30 μg for the stable flow-FFF sample, compared to 200 μg for previous SEC separations that show no similar instabilities.

Narrow fractions of SWNT/DNA were prepared by SEC as reported elsewhere.[2,17,18] Figure 2 shows absorbance at 690 nm for 12 different fractions and unfractionated SWNT/DNA. Absorbance of each fraction and unfractionated SWNT/DNA is normalized by its area to illustrate relative breadth of the distributions. As indicated in Figure 2, different lengths of SWNTs (i.e., different fractions) clearly show different elution times and have narrower distributions than that of unfractionated SWNT. Note that the fraction number is in reverse order of their lengths due to the SEC separation mechanism. The width of the elution time peaks decreases as the fraction number increases. The original SEC fractions were collected at equal time intervals in a mixed bed column set. Such a column set is expected to separate as a logarithm of molar mass over the range of fraction collection resulting in similar polydispersity for each fraction shown. Figure 3 is a plot of peak position from flow-FFF for SEC fractions. The peaks are better resolved for the longer SEC fractions than for the shorter ones as is evident by the greater slope of the line. This is further evidence that the longer SWNTs are fractionated more efficiently with the flow profile used in this study. Because the flow profile used in flow-FFF separation can be programmed in a complicated manner, another flow profile may separate with a different relative shape of the curve shown in Figure 2.

Molar Mass and Length. From online MALS and UV−vis spectroscopy, one can obtain the Rayleigh ratio and concentration of SWNT as a function of time. Concentration at each time is calculated from absorbance by using an extinction coefficient for SWNTs of 26 000 mL/g cm from a separate measurement, as shown in our previous SEC study.[2,17,18] Because we measure absorbance at 690 nm where length-dependent optical effects are minimal,[2] absolute absorbance can be directly converted to concentration. In order to obtain molar mass and length from the scattering and absorbance measurements, one should correlate the measurements with molar mass and length. Under an assumption of dilute solution, a correlation between those parameters can be described by[19,20]

(19) Roe, R.-J. *Methods of X-ray and Neutron Scattering in Polymer Science*; Oxford University Press: New York, 2000.
(20) Tanford, C. *Physical Chemistry of Macromolecules*; John Wiley & Sons: New York, 1967.

$$R_\theta = KcMP(qL) \quad (1)$$

where R_θ is the Rayleigh ratio at scattering angle θ, M is molar mass, c is concentration, and $P(qL)$ is the form factor of the SWNT. Here K is an optical constant and q is the magnitude of the scattering vector defined by $4\pi n_0 \sin(\theta/2)/\lambda_0$, where n_0 is the refractive index of the medium, λ_0 is the wavelength of incident light, and L is the SWNT length. For a monodisperse and isotropic rod, a well-known correlation is[19,20]

$$\frac{R_\theta}{K^*c} = M\left[\frac{2}{qL}\int_0^{qL}\frac{\sin t}{t}\,\mathrm{d}t - \frac{\sin^2(qL/2)}{(qL/2)^2}\right] \quad (2)$$

Here $K^* = 4\pi^2 n_0^2(\mathrm{d}n/\mathrm{d}c)^2\lambda_0 N_A^{-1}$, where N_A is Avogadro's number.

However, SWNTs are known to possess significant optical anisotropy, such that one should use a similar relationship for a monodisperse and anisotropic rod in order to obtain a more accurate mass and length. Utilizing previous studies on the optical anisotropy and dielectric response of SWNT/DNA suspensions,[21,22] we obtain the following relation:

$$R_\theta = \left(\frac{\pi^2 {n_0}^4}{\rho^2 {\lambda_0}^4 N_A}\right)cM[I_1 + I_2] \quad (3)$$

where ρ denotes the mass density of SWNT.[17] Here I_1 and I_2 represent isotropic and anisotropic parts of the scattering function and are described by

$$I_1 = 0.48\left[\frac{2}{qL}\int_0^{qL}\frac{\sin t}{t}\,\mathrm{d}t - \frac{\sin^2(qL/2)}{(qL/2)^2}\right] \quad (4)$$

and

$$I_2 = \frac{8.57}{4\pi}\int_0^{2\pi}\mathrm{d}\phi\int_0^{\pi}\mathrm{d}\theta\,\sin\theta\cos^2\phi\left[\frac{\sin^2(qL\cos\phi\sin\theta/2)}{(qL\cos\phi\sin\theta/2)^2}\right] = \frac{2.143}{(qL/2)^3}\left[-qL + \frac{qL}{2}\cos qL + \frac{1}{2}\sin qL + 2\left(\frac{qL}{2}\right)^2\int_0^{qL}\frac{\sin t}{t}\,\mathrm{d}t\right] \quad (5)$$

for CoMoCat SWNTs at 690 nm excitation. With the use of a nonlinear least-square scheme (Levenberg−Marquardt method)[23] with 1.0 g/mL for the mass density of SWNT, we obtain the molar mass and length for unfractionated SWNT/DNA at each time which minimizes the χ^2 of the fit [i.e., eq 3]. Figure 4 shows molar mass and length distributions of unfractionated SWNT along with the normalized absorbance at 690 nm. The MALS signal strength is weak due to the low concentration necessary for flow-FFF separation. Figure 4 is a plot of M and L as a function of elution time with representative error bars showing 1 standard deviation. Data are not included when the standard deviation exceeds the measured parameter. Because the relative uncertainty of the molar mass is smaller than that of the rod length, the data range of the plotted molar mass extends to earlier elution times.

The slopes of the rod length and the molar mass with time are large for the smaller SWNTs which elute at the earliest times. This is characteristic of inefficient separation with time and is consistent with the conclusion based on the slope of the curve in Figure 3 as stated previously. The range of the peak positions from the SEC fractions are shown for comparison. During the upper size limits of this range, the molar mass and rod length run parallel which would give $L \propto M^{1.0}$ characteristic of a rodlike structure. At 55 min, the cross-flow ramp decreases to zero and all material elutes. The large upturn of molar mass and rod length at this point is due to small quantities of very large material. It is at the maximum size limit of the MALS instrumentation and it cannot be determined if it is long SWNTs or SWNT bundles. This large material elutes well after the longest SWNT SEC fraction elutes. It may represent separation in a size region inaccessible to SEC separations.

Figure 5 is a plot of flow-FFF elution time as a function of hydrodynamic diameter. The red squares are the results for polystyrene latex spheres with diameters of 19, 35, 92, 300, 600, and 990 nm. There is a continuous increase in elution time until a maximum is reached at about 55 min. This maximum is characteristic of when the cross flow goes to zero and all the remaining material elutes by this time. It is also characteristic of approaching a steric limit at which size the elution is no longer controlled by diffusion of the spheres. At this point, the spheres roll along the surface and eventually the largest spheres elute earlier.[24] However, as described in an earlier section, the rodlike structure of the dispersed SWNTs used in this study (<1 μm) is expected to align parallel to the accumulation wall and thus not demonstrate this particular steric limit.

Because we have used fractions obtained from our previous SEC studies,[2,17,18] they can be compared to hydrodynamic diameters from the SEC calibration of hydrodynamic volume. The SEC fractions are plotted in Figure 5 as blue circles giving elution time as a function of hydrodynamic diameter measured from SEC. Similar to our calibration with polystyrene latex particles, a hydrodynamic diameter of each fraction was obtained by using 10 different polystyrenes, 580 to 7 500 000 g/mol, in tetrahydrofuran (THF) and using "universal calibration".[25] The latex spheres and the SEC fractions form a composite curve with an overlap of hydrodynamic diameters over approximately one decade.

Even the longest SEC fraction elutes well before the maximum elution time seen for the spheres. The longest SEC fraction was taken at the exclusion limit of the column set above which longer SWNTs could not be resolved or do not pass through the column. This suggests that flow-FFF separation of SWNTs may be capable of resolving SWNTs with lengths over a much wider size range

(21) Hobbie, E. K. *J. Chem. Phys.* **2004**, *121*, 1029.
(22) Fagan, J. A.; Simpson, J. R.; Landi, B. J.; Richter, L. J.; Mandelbaum, I.; Bajpai, V.; Ho, D. L.; Raffaelle, R.; Hight Walker, A. R.; Bauer, B. J.; Hobbie, E. K. *Phys. Rev. Lett.* **2007**, *98*, 147402.
(23) Press, W. H.; Teukolsky, S. A.; Vetterling, W. T.; Flannery, B. P. *Numerical Recipes in FORTRAN*; Cambridge University Press: New York, 1994.
(24) Schimpf, M.; Caldwell, K.; Giddings, J. C. *Field-Flow Fractionation Handbook*; Wiley-Interscience Publication: New York, 2000.
(25) Mori, S.; Barth, H. G. *Size Exclusion Chromatography*; Springer: Berlin, Germany, 1999.

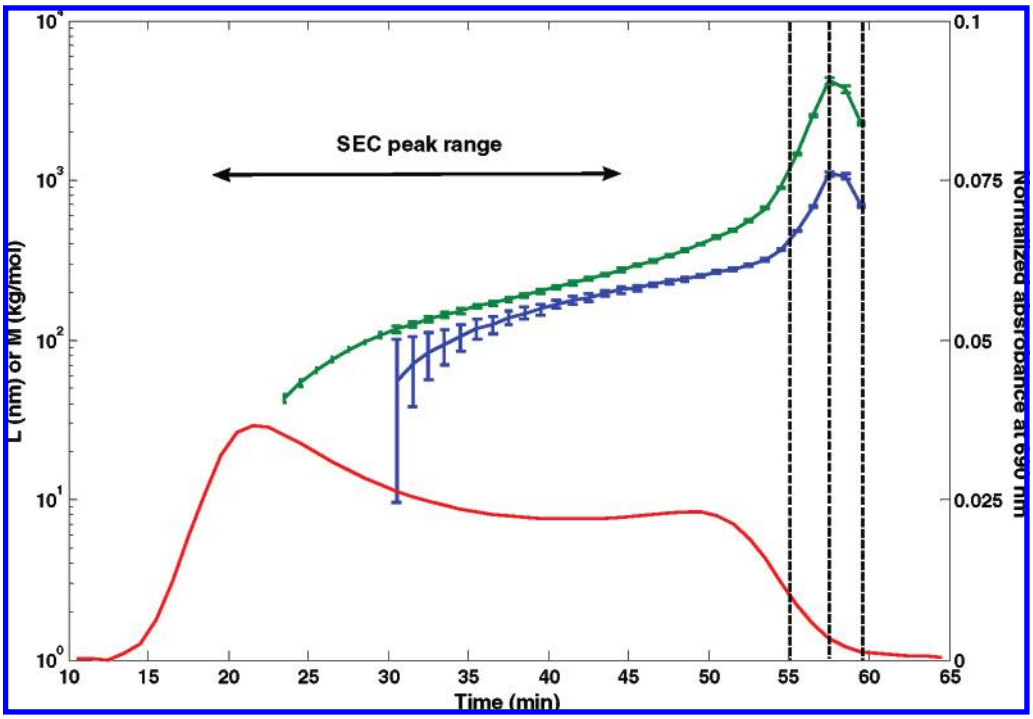

Figure 4. Molar mass and length distributions of unfractionated SWNT/DNA along with the normalized elution profile. Red, green, and blue lines denote normalized absorbance, molar mass, and length, respectively, and the error bars for molar mass and length represent one standard deviation. Molar mass and length for unfractionated SWNT are plotted only when the relative uncertainty is less than 50%. This eliminates data at early times due to very weak scattering signals. The upturn in molar mass and length starts near the time that the cross flow goes to zero (about 55 min) and represents <10 mass % of the sample.

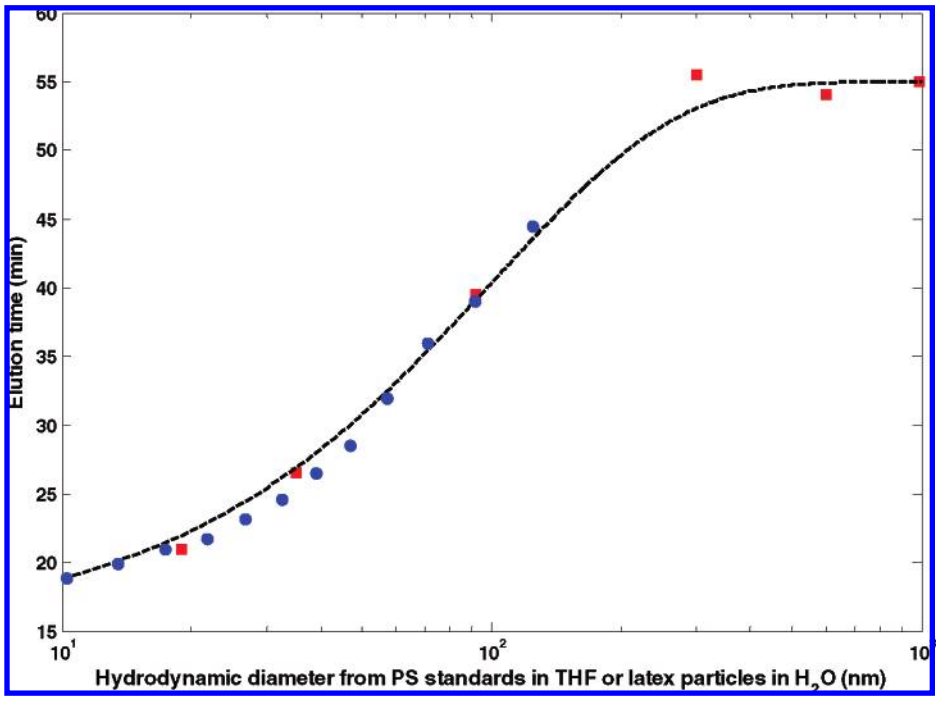

Figure 5. Flow FFF elution times for six different polymer latex particles, 19, 35, 92, 300, 600, and 990 nm in diameter, under identical experimental conditions as those for the SWNT SEC fractions (red squares). Blue circles denote elution times as a function of hydrodynamic diameter for the SWNT SEC fractions based on polystyrene standards with THF calibration. The curve denotes the fit based on eqs 6−8.

than is capable by SEC. The upturn in molar mass and rod length seen in Figure 4 occurs during this elution time, and flow-FFF is capable of size resolution in this range.

A fit was made of the elution times of the spheres by normal mode theory for flow-FFF.[24] A sphere with diameter d in a fluid with viscosity μ at temperature T has a diffusion coefficient, D, which is

$$D = \frac{kT}{3\pi\mu d} \tag{6}$$

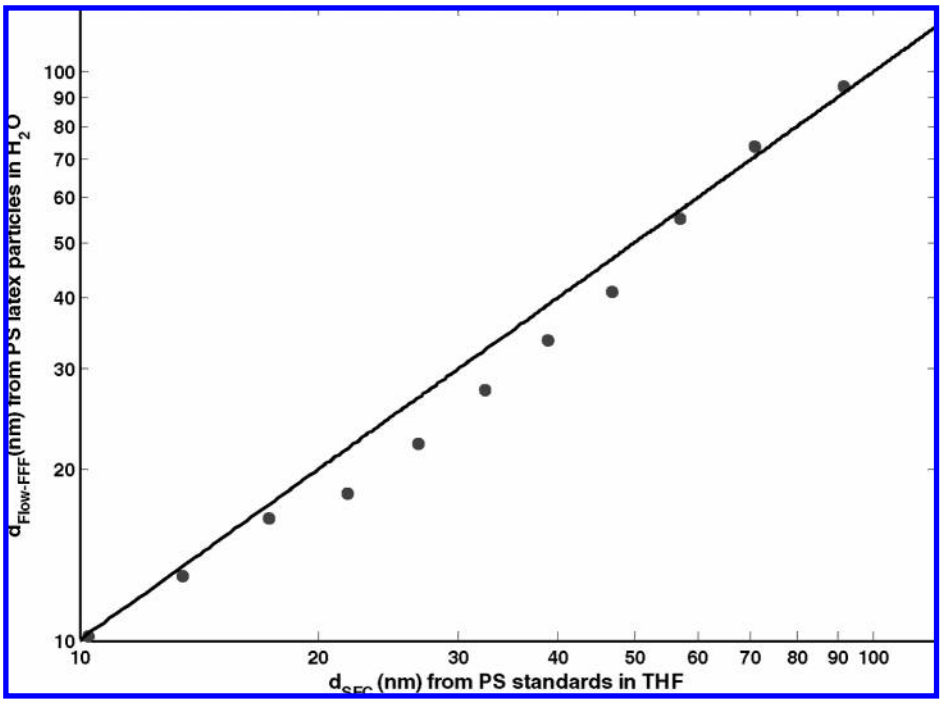

Figure 6. The correlation between hydrodynamic diameters from both flow-FFF and SEC for 12 different fractions. Hydrodynamic diameters for flow-FFF, $d_{flow-FFF}$, are obtained from polystyrene latex particles of known diameters under aqueous solution and those for SEC, d_{SEC}, are from polystyrene standards of known molecular weights in tetrahydrofuran (THF) solvent. The line corresponds to the condition that two hydrodynamic diameters are identical, i.e., $d_{flow-FFF} = d_{SEC}$.

A separation parameter, $\tilde{\lambda}$, is defined with volumetric cross flow, V_C, in a channel with volume V_0 and channel separation w.

$$\tilde{\lambda} = \frac{V_0 D}{V_C w^2} \tag{7}$$

The retention ratio, R, and the elution time, t, are calculated for normal mode separations with channel flow V as

$$R = 6\tilde{\lambda}\coth\left(\frac{1}{2\tilde{\lambda}}\right) - 12\tilde{\lambda}^2 = \frac{V_0}{Vt} \tag{8}$$

Equations 6−8 were used to fit the elution of the spheres, plotted as a dashed curve in Figure 5. Whereas the curve was fit only to the latex sphere data, it also passes through the SEC fraction data even outside of the fit range. This demonstrates that calibration of flow-FFF with latex spheres can be used for analysis of SWNT elution data.

Figure 6 compares the SEC fraction hydrodynamic diameters (from calibration with PS in THF) with the same fractions separated with flow-FFF (from calibration with latex spheres). The hydrodynamic volumes measured by SEC and flow-FFF agree well even though the calibrations are made with quite different standards.

Calculation of Rod Lengths from Hydrodynamic Volumes. With the use of the calibration curve shown in Figure 5, one can obtain lengths of the SEC fractions. This was done by converting the hydrodynamic volumes from latex calibration to rod lengths from an appropriate hydrodynamic model. Two representative models of rodlike SWNTs were used. The first method, modeling the SWNT as an ellipsoidal particle, is to equate a translational diffusivity, D, of a sphere with diameter d, ($D = kT/3\pi\mu d$) with an effective translational diffusivity of ellipsoidal particle (D_{el}) averaged over all orientations (i.e., based on a free-rotating ellipsoidal particle), which can be described by[26]

$$D_{el} = \frac{kT}{6\pi\mu a\sqrt{1-\left(\frac{b}{a}\right)^2}}\ln\left[\frac{1+\sqrt{1-\left(\frac{b}{a}\right)^2}}{\left(\frac{b}{a}\right)}\right] \tag{9}$$

where $2a$ is the length of the major axis of the ellipsoidal particle and $2b$ is the length of the minor axis. The second method is to equate a friction coefficient for a sphere ($f = 3\pi\mu d$) with that of a rodlike particle averaged over all angles (f_{ave}). Considering slender body theory, which is a good approximation for SWNTs due to the large aspect ratio, friction factors for the longitudinal ($f_{||}$) and transverse ($f_{\perp}$) directions of a rodlike particle are

$$f_{||} = 4\pi\mu L\left[\frac{\epsilon(1+0.307\epsilon)}{1-0.5\epsilon} + 0.119\epsilon^3\right] \tag{10}$$

$$f_{\perp} = 8\pi\mu L\left[\frac{\epsilon(1+0.307\epsilon)}{1+0.5\epsilon} + 0.426\epsilon^3\right] \tag{11}$$

where $\epsilon = 1/\ln(\gamma/2)$.[27] Then, an averaged friction coefficient may be obtained as $f_{ave} = (f_{||} + 2f_{\perp})/3$. Note that the longitudinal and transverse directions here are with respect to the cross-flow

(26) Perrin, F. *J. Phys. Radium* **1936**, *7*, 1.
(27) Batchelor, G. K. *J. Fluid Mech.* **1970**, *44*, 419.

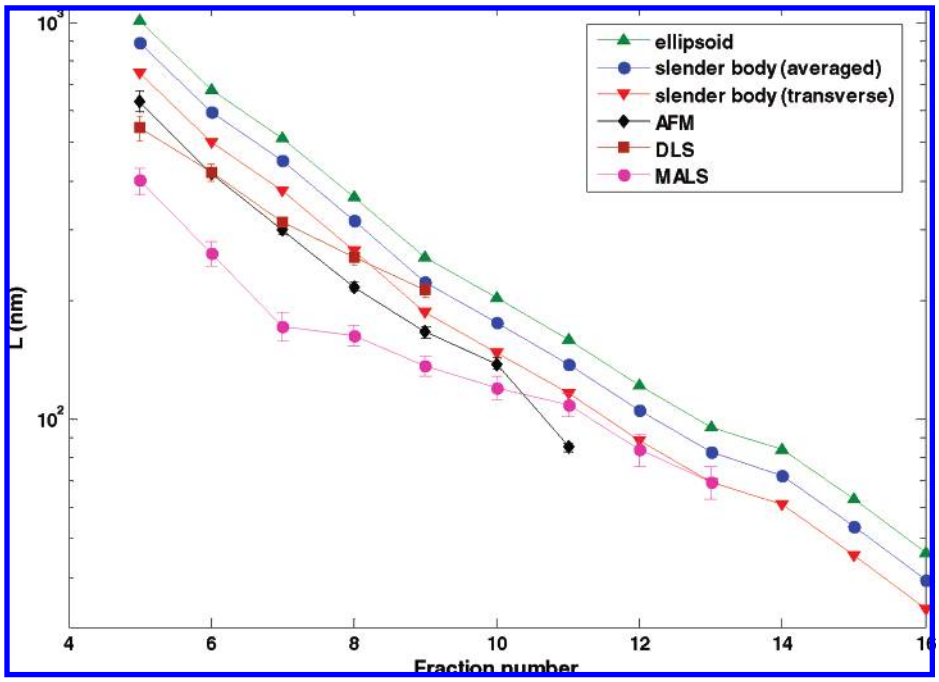

Figure 7. Lengths of SWNTs for 12 fractions from calibration with polymer latex particles along with those from previous AFM and DLS measurements (fractions 5−9) and current UV−vis and scattering measurements (fractions 5−13). ▲, blue ●, and ▼ are those from the calibration. ▲ are lengths obtained from an ellipsoid approximation. Both ● and ▼ are lengths from the slender body approximation; blue ● are based on the friction coefficient averaged over all angles and ▼ are based on the transverse friction coefficient (i.e., aligned to the wall). ♦ and ■ denote lengths from AFM and DLS, respectively. Magenta ● represent lengths from absorbance and scattering measurements for the fractions. The error bars for the AFM and DLS data represent 1 standard deviation.

direction because the uniform velocity field (i.e., the cross flow) is a driving force to change the center-of-mass position of the rodlike particle leading to the length separation.

Figure 7 shows lengths of fractions estimated from calibration with polymer latex particles (i.e., based on D_{el}, f_{ave}, and $f_{\perp}$), along with those from AFM and DLS. (fractions 5−9) and from MALS (fractions 5−13). The lengths from MALS for the fractions are consistently smaller than those from AFM and DLS, which was also seen in a previous SEC study.[2,17,18] The lengths from DLS are obtained from rotational relaxation times by use of the rotary diffusivity of a rodlike model as described elsewhere.[2] The difference between the three measurements might be due to an intrinsic experimental uncertainty for each method. The lengths from hydrodynamic volumes are consistently larger than those from AFM and DLS.

As seen in Figure 7, estimated lengths from slender body theory are more reasonable than those from the ellipsoid approximation, when compared to those with AFM, DLS, and MALS. Whereas estimations from the two different methods become similar to each other as SWNT length decreases, Figure 7 suggests that the slender body approximation is more appropriate to describe the dynamics of SWNTs above the $O(100)$ nm range of length.

Figure 7 shows that the estimated lengths from the averaged friction coefficient, f_{ave}, have larger deviations than those obtained from the transverse friction coefficient, $f_{\perp}$, compared to those with AFM and DLS above 200 nm in length. This implies that a balance between the friction coefficients of the transverse direction for a rod and a sphere would be more appropriate for that length scale. This, in turn, is qualitatively in accordance with the simple scaling argument that SWNTs start to align perpendicular to the cross-flow direction (i.e., parallel to an accumulation wall of the channel) at around 600 nm in length due to a significant "effective" rotary Peclet number, as pointed out in an earlier section.

Relative SWNT Size Distributions. The three primary methods of producing varied SWNT sizes are SEC, flow-FFF, and high-energy fracture through extended sonication. Other size separation methods such as electrophoresis may prove valuable but are presently not being used for preparative SWNT separations. The relative merits of the different separation schemes can be examined by analyzing fractions through multiple techniques. Figure 2 is an example of this procedure with flow-FFF being used to separate SEC fractions. Whereas the peaks are clearly separated in a consistent manner as demonstrated in Figure 3, the distributions in Figure 2 have overlap in their shoulders. This broadening of the elution times of a SEC fraction may be a consequence of slightly poorer resolution of flow-FFF compared to SEC.

Figure 8 shows absorbance at 690 nm of three different sonication times, 2, 14, and 27 h, in the preparation of SWNT/DNA dispersions. Extended sonication times can fracture the SWNTs, producing increasingly shorter SWNTs with longer times. There is a clear shift in the chromatograms with sonication time to earlier separation times showing a loss of longer SWNTs and a gain of shorter ones. Whereas the fracture process clearly changes the average length of the SWNTs, the distribution of lengths is still quite broad. This can be seen by comparing them to SEC fractions. Figure 8 shows the flow-FFF separation of an SEC fraction that has a peak in a similar position as the batch is sonicated for 27 h. The SEC fraction is considerably narrower

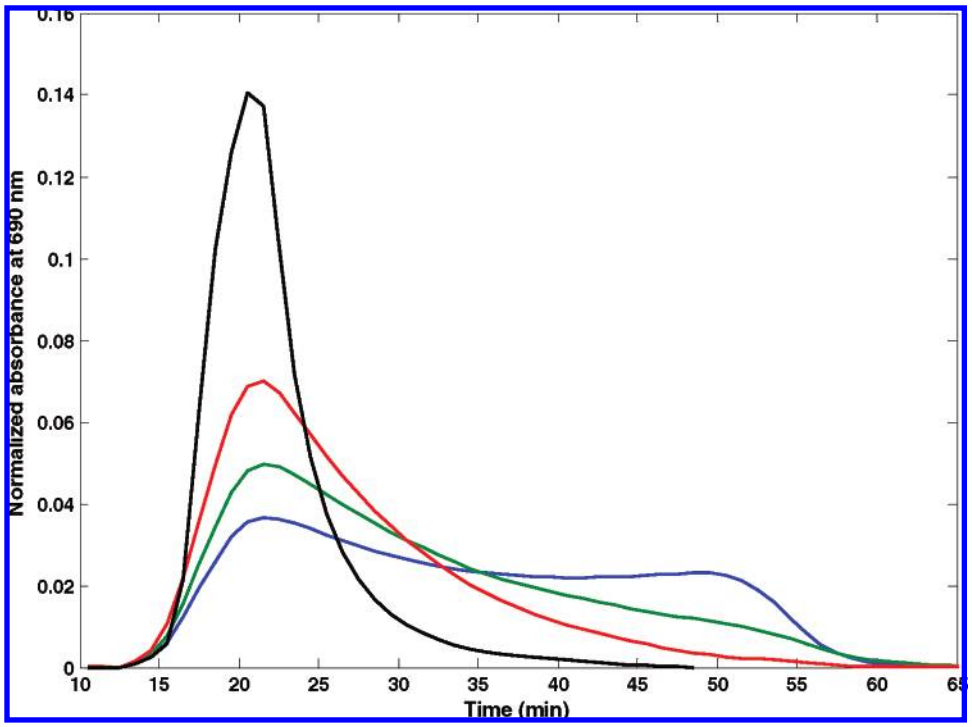

Figure 8. Flow-FFF elution profiles for SWNT/DNA suspensions having three different sonication times and SEC fraction 15. Blue, green, and red lines represent 2, 14, and 27 h of sonication times, respectively. The black line is SEC fraction 15. The breadths of the distributions with time demonstrate that the products of sonication fracture have significantly broader size distributions than flow-FFF fractions.

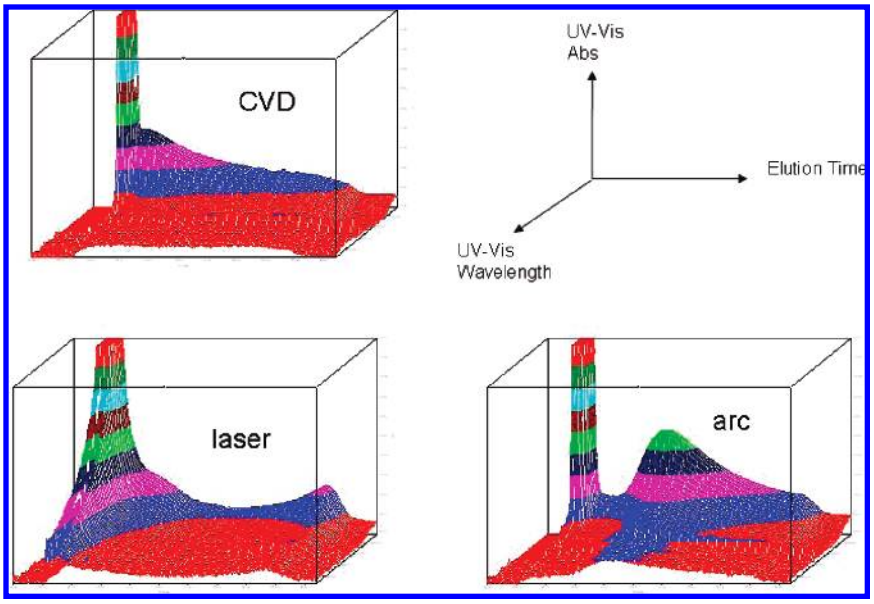

Figure 9. Flow-FFF elution profiles of CVD, laser, and arc SWNTs. Full spectra were taken with a photodiode array every second. Axis left to right, elution time 10−65 min; axis bottom to top, UV−vis absorbance 0−0.02; axis back to front, UV−vis wavelength 220−650 nm. The high peak to the left of the figures is unattached DNA. The remainder of the spectra are characteristics of SWNTs. These three plots show clearly distinct features of each batch of SWNT.

than the fractured sample. Therefore, whereas fracturing processes such as extended sonication can produce samples with varied average lengths, both SEC and flow-FFF can produce much narrower distribution fractions.

Figures 2 and 8 also demonstrate that flow-FFF offers a convenient analytical method of comparing SWNT size distributions. It clearly demonstrates the effectiveness of various methods of modifying SWNT sizes, but flow-FFF is also effective in comparing different SWNT types or different SWNT batches. As an example, Figure 9 is a plot of flow-FFF separations of three different SWNT synthetic types, chemical vapor deposition (CVD), laser ablation SWNTs, and electric arc. Full spectra were taken once every second with a PDA, and 3D images were constructed as a function of elution time and are plotted as indicated in Figure 9. There is clearly enough sensitivity in PDA measurement of the UV−vis spectrum of the eluting SWNT/DNA to identify the SWNT type and length distribution for a uniformity analysis for quality control.

CONCLUSIONS

Flow-FFF was used to separate single wall carbon nanotubes in aqueous dispersions. Size separated fractions obtained from size exclusion chromatography were compared to unfractionated samples, and they demonstrated efficient separations. Calibrations with latex particles of known sizes were compared to elution times of SEC fractions. The hydrodynamic sizes from flow-FFF and SEC were in general agreement. Online MALS identified late-eluting components from unfractionated SWNTs as being considerably larger than SWNTs separated by SEC.

Hydrodynamic models were applied to flow-FFF to estimate the length of rods or ellipsoids that had similar elution characteristics. The calibrations with two different methods indicate that slender body theory describes the dynamics of SWNTs more closely than an ellipsoid approximation does. The rod lengths were consistent with other measurements such as AFM, DLS, and MALS, though slightly longer lengths were estimated.

As an analytical tool, flow-FFF is capable of estimating subtle differences in SWNT size distributions. The change in size distributions caused through SWNT fracture is easily seen, but the size distributions of such materials are considerably broader than either SEC or flow-FFF fractions. Flow-FFF of dispersions of SWNTs synthesized by different processes shows considerably different size distributions and spectra demonstrating that it may prove to be a simple method of SWNT identification and quality assessment.

Received for review November 16, 2007. Accepted January 20, 2008.

AC7023624